

# NONLINEAR SPECTRAL MIXING MODELS FOR VEGETATIVE AND SOIL SURFACES

Christoph C. Borel and Siegfried A.W. Gerstl

Space Science & Technology Division

Los Alamos National Laboratory, MS D436

Los Alamos, New Mexico 87545, USA

August 25, 1994

## **Abstract**

In this paper we apply an analytical solution of the radiosity equation to compute vegetation indices, reflectance spectra and the spectral bi-directional reflectance distribution function for simple canopy geometries. We show that nonlinear spectral mixing occurs due to multiple reflection and transmission from surfaces. We compare radiosity-derived spectra with single scattering or linear mixing models. We also develop a simple model to predict the reflectance spectrum of binary and ternary mineral mixtures of faceted surfaces. The two facet model is validated by measurements of the reflectance.

## **1 Introduction**

Vegetation indices have been widely used and related to biophysical canopy parameters such as leaf area index (e.g. Goel (1988), Asrar (1989) and Baret and Guyot (1991)). They are usually based on ratios of two measured radiances that relate to spectral reflectances from two spectral bands as shown by Tucker (1979) or a combination of multiple bands, see Kauth and Thomas (1976) and Jackson (1983). Operational satellite sensors such as Landsat TM, Spot and AVHRR have multiple spectral bands which are used not only to classify pixels into distinct surface classes e.g. vegetation, bare soil, water etc., but also to estimate fractions of basic classes within each pixel (e.g. Huete (1986), Satterwhite and Henley (1987), Smith, Ustin, Adams and Gillespie (1990, part I and II) and Roberts (1991). With the deployment of airborne hyper-spectral sensors such as the Airborne Imaging Spectrometer

(AIS) (Vane and Goetz (1988)) and the Airborne Visible/Infrared Imaging Spectrometer (AVIRIS) (Green (1991)) and projected sensors such as the High-Resolution Imaging Spectrometer (HIRIS) (Goetz (1987) and Dozier and Goetz (1989)) and the Moderate Resolution Imaging Spectrometer (MODIS) (Salomonson, Barnes, Maymon, Montgomery and Ostrow (1989)) in the EOS program we must develop new and physically based scattering models to take advantage of the hyper-spectral information.

Linear spectral factor analysis or un-mixing theory has been widely used to compute the abundance or percentage of soil or mineral components in a surface cover, e.g. Huete, Jackson and Post (1985), Huete (1986), Smith, Ustin, Adams and Gillespie (1990), Roberts (1991). With the Airborne Visible/Infrared Imaging Spectrometer (AVIRIS) (Green (1991)) it is now possible to test various spectral models.

Others observed that no linear combination of spectra can fully represent the measured composite scene spectra and that residuals can be quite large, see Roberts, Smith and Adams (1990) and Roberts, Smith, Adams and Gillespie (1991). The residual or remaining part has been attributed to the “shade” in the scene (Roberts (1991)) and is assumed to be a constant. Measured reflectances for broad leaf trees like sugar maple show that the NIR reflectance at the branch level is higher than at the leaf level (Williams (1991)). We will show that this effect is due to multiple reflections between leaves.

In this paper we will present a novel method to compute the reflectance spectrum and the spectral bi-directional reflectance distribution function for two simple canopy geometries. The method used is based on the radiosity method, see Hottel and Sarofim (1967), Borel, Gerstl and Powers (1991) and Gerstl and Borel (1991), and is in principle applicable to many complex surface types and also volumetric scattering, see Rushmeier and Torrance (1987) and Borel and Gerstl and Borel (1991).

To illustrate the nonlinear spectral mixing effect we start with a simple model, a single-layer of vegetation above soil. The model used in this paper has already been described in detail in Borel, Gerstl and Powers (1991) but will be briefly summarized. We demonstrate that the nonlinear spectral mixing is due to multiple reflections and transmissions between the leaf layer and soil.

Next, a layered canopy model is described and used to compute vegetation indices and the spectral BRDF using analytical solutions derived in Borel, Gerstl and Powers (1991).

The method presented can also be applied to rough surfaces and in the final section a simple model for rough soil is developed and validated. Other researchers have noted that nonlinear spectral mixing occurs when two or more substances are mixed and the reflectance spectrum is measured, see Nash (1974), Hapke (1981) and Johnson (1983). We compute the reflectance of binary and ternary mineral mixtures using the radiosity method.

## 2 Nonlinear Mixing in a Single Layer Canopy using Radiosity

In this section we repeat some of the derivations from Borel, Gerstl and Powers (1991) because there was a typographical error in one of the radiosity equations, which caused the analytical solution to be wrong as well. Analytic expressions for the BRDF in the hot spot direction and away from it are also derived. A simple linear reflectance model for soil is used to compute the reflectance. Vegetation indices are computed using two wavelengths in the red and near infrared part of the spectrum.

### 2.1 Review of the Single Layer Radiosity Model

For a single-layer canopy of horizontal and non-overlapping Lambertian disks above a Lambertian surface, see Figure 1, the three radiosity equations can be written down by heuristic arguments. From Borel, Gerstl and Powers (1991) we obtain equations for the layer-averaged radiosity of the top surface of the leaf layer ( $B_1$ ), the underside ( $B_2$ ) and the ground surface ( $B_3$ ) :

$$\begin{aligned} B_1 &= \rho \, lai \, E_0 + \tau \, lai \, B_3 \\ B_2 &= \tau \, lai \, E_0 + \rho \, lai \, B_3 \\ B_3 &= \rho_s (1 - lai) E_0 + \rho_s B_2, \end{aligned} \tag{1}$$

where  $E_0$  is the total incident solar power per unit area in  $[Wm^{-2}]$ ,  $lai$  is the leaf area index of a leaf layer without overlapping leaves in  $[m^2m^{-2}]$ ,  $\rho$  and  $\tau$  are the hemispherical reflectance and transmittance of the leaves, and  $\rho_s$  is the soil reflectance. Note that in this case the  $lai$  is also equal to the green fractional cover.

The analytical solution of the set of linear equations (1) is :

$$B_1 = E_0 \, lai \, \rho + E_0 \, lai \, \tau \, \rho_s \left[ \frac{1 + lai(\tau - 1)}{1 - \rho \rho_s lai} \right]$$

$$\begin{aligned}
B_2 &= E_0 \, lai \left[ \frac{\tau + \rho \rho_s (1 - lai)}{1 - \rho \rho_s lai} \right] \\
B_3 &= E_0 \, \rho_s \left[ \frac{1 + lai(\tau - 1)}{1 - \rho \rho_s lai} \right].
\end{aligned} \tag{2}$$

## 2.2 Computing the Spectral Bi-Directional Reflectance Distribution Function (BRDF) for a Single Layer Canopy

The BRDF of a single-layer canopy is given by adding all visible surface radiosities for a given sun angle  $(\theta_i, \phi_i)$  and view direction  $(\theta_r, \phi_r)$  or :

$$\begin{aligned}
f(\theta_i, \phi_i; \theta_r, \phi_r) &= \frac{1}{E_0} \frac{1}{\pi} [ P_{leaf}^{sunlit}(\theta_r, \phi_r) B_{leaf}^{sunlit} + P_{soil}^{sunlit}(\theta_r, \phi_r) \\
&\quad + B_{soil}^{sunlit} P_{soil}^{shade}(\theta_r, \phi_r) B_{soil}^{shade} ],
\end{aligned} \tag{3}$$

where the radiosity on a sunlit leaf is given by:

$$B_{leaf}^{sunlit} = \frac{B_1}{lai} \tag{4}$$

and the radiosities on the sunlit and shaded soil areas are given by:

$$B_{soil}^{sunlit} = \rho_s E_0 + \rho_s B_2 \tag{5}$$

and

$$B_{soil}^{shade} = \rho_s B_2. \tag{6}$$

By definition of the leaf area index the probability of seeing a sunlit leaf is :

$$P_{leaf}^{sunlit} = lai. \tag{7}$$

One can show that the BRDF of a single layer of horizontal leaves asymptotically reaches constant value away from the hot spot  $(\theta_r \neq \theta_i, \phi_r \neq \phi_i)$  and peaks in the hot spot direction  $(\theta_r = \theta_i, \phi_r = \phi_i)$ , see Borel, Gerstl and Powers (1991). For the hot spot direction no shaded ground is visible therefore :

$$P_{soil}^{shade/hotspot} = 0, \tag{8}$$

and

$$P_{soil}^{sunlit/hotspot} = 1 - lai. \tag{9}$$

Away from the hot spot direction the probability of seeing sunlit ground is given by the product of the probability of sunlit ground and the probability of seeing through the leaf

layer or :

$$P_{soil}^{sunlit} = (1 - lai)^2, \quad (10)$$

and the probability of seeing shaded soil is given by the product of shaded ground area density and the probability of seeing through the leaf layer or :

$$P_{soil}^{shade} = lai (1 - lai). \quad (11)$$

Using eqs. (4)-(11) in eq. (3) we get for the hot spot direction :

$$f(\theta_r = \theta_i, \phi_r = \phi_i) = \frac{1}{E_0} \frac{1}{\pi} [B_1 + \rho_s (1 - lai) (E_0 + B_2)], \quad (12)$$

and for the directions away from the hot spot :

$$\begin{aligned} f(\theta_r \neq \theta_i, \phi_r \neq \phi_i) &= \frac{1}{E_0} \frac{1}{\pi} [B_1 + (1 - lai) B_3] \\ &= \frac{1}{E_0} \frac{1}{\pi} [B_1 + \rho_s (1 - lai)^2 E_0 + \rho_s (1 - lai) B_2]. \end{aligned} \quad (13)$$

In the solution of the radiosity equations (2) we find terms of the form :

$$\frac{1}{1 - \rho \rho_s lai} \quad (14)$$

represent multiple reflections between the leaf layer and soil. Eq. (14) is a quadratic summation:

$$\frac{1}{1 - \rho \rho_s lai} = 1 + \rho \rho_s lai + (\rho \rho_s lai)^2 + (\rho \rho_s lai)^3 + \dots \quad (15)$$

and thus the BRDF's in eqs. (12) and (13) are a nonlinear function of the reflectance spectra of the vegetation and the soil. Thus we define a nonlinear spectral mixing model as a model which contains products of reflectances. It should be noted that eqs. (12) and (13) can be solved analytically for  $lai$ ,  $\rho$  and  $\rho_s$ .

### 2.3 Numerical Results for the Single-Layer Canopy

In this subsection we will compare the classic linear mixture model and the radiosity mixture model with some measured leaf spectra (Staenz (1991)) of cotton plants. The conical/bi-hemispherical spectral reflectance and transmittance of a cotton leaf was measured shortly after removing the leaf from a mature cotton plant. The instrument, a spectro-radiometer (LICOR-1800), measured the reflectance and transmittance from 300 nm to 1100 nm with a useful range from 400 nm to 1100 nm. The measured spectra are shown in Figure 2. Notice

that we use the left vertical axis for the reflectance curve and the right vertical axis for transmittance. The vertical distance between the curves indicates the amount of absorption in a leaf which is small for wavelengths greater than 730 nm. To make the nonlinear effects on the canopy BRDF more easily understood we approximate the soil reflectance by a linear function :

$$\rho_s(\lambda) = a + b \frac{(\lambda - 400)}{700} \quad (16)$$

where  $\lambda$  is the wavelength in *nm*. The coefficients  $a$  and  $b$  were chosen to approximate a background of brown leaf litter or soil. The coefficients for the ground reflectance were  $a = 0.2$  and  $b = 0.6$ . We also varied the leaf area index *lai* from 0.0625 to 0.9375 in steps of 0.125 and the results are shown in Figure 3.

The linear mixing model assumes that the fraction of visible leaves is given by the *lai* and that the fraction of visible sunlit ground is given by  $(1 - lai)^2$  for a viewing direction far away from the hot spot direction. Thus the linear mixing BRDF is given by:

$$f(\theta_r \neq \theta_i, \phi_r \neq \phi_i) = \frac{1}{\pi} [lai \rho + (1 - lai)^2 \rho_s]. \quad (17)$$

Note that this linear (no products of reflectances) mixing model takes shading of the ground into account. Usually the shadow fraction is not taken into account and only recently Roberts, Adams and Smith (1990) and Roberts (1991) have used the shadow fraction in spectral mixture analysis as an additional endmember. In the hot spot direction, the BRDF dominates all displayed curves because no shadows are visible. For low reflectances (e.g. in the visible) the higher order terms in eq. (15) are negligible. In the region of the green reflectance peak near 550 nm there is a small difference between the linear mixing model and the radiosity mixing model. For high reflectances (e.g. in the near infrared,  $\lambda > 700$  nm, for  $\rho > 0.3$  and  $\rho_s > 0.3$ ) the higher-order terms contribute more to the calculated radiosity and therefore increase the BRDF significantly. The difference between the two models is a function of the leaf area index and reaches a maximum for an *lai* of about 0.5. The hot spot BRDF is always higher than the off hot spot BRDF and the difference increases with increasing leaf and/or soil reflectance. In the near infrared the radiosity method yields BRDF's almost twice as high as with the linear mixing model which was confirmed experimentally by Roberts (1992).

## 2.4 Vegetation Indices and Nonlinear Mixing

Vegetation indices have been widely used and related to bio-physical parameters such as the total leaf area index ( $LAI$ ), see e.g. Huete, Jackson and Post (1985); Goel (1988); Asrar (1989); Smith, Ustin, Adams and Gillespie (1990); Cihlar, St-Laurent and Dyer (1991); Baret and Guyot (1991) and many others. The vegetation index has been shown by Jasinski (1990) to depend also on canopy cover, soil albedo, solar and view angle and pixel scale. From our model it is clear that the relationship between a vegetation index,  $LAI$  and the vegetation and soil reflectances is nonlinear (see eq.(15)). We have computed various vegetation indices, e.g. Baret and Guyot (1991), as shown in Table 1.

**Table 1** Some commonly used vegetation indices

Vegetation Index	Formula
Normalized difference vegetation index (NDVI)	$(NIR - RED)/(NIR + RED)$
Vegetation index (VI)	$NIR/RED$
Soil-adjusted vegetation index (SAVI)	$\frac{3}{2}[(NIR - RED)/(NIR + RED + 0.5)]$

For the RED reflectance we chose  $\lambda = 650 \text{ nm}$  and for the near infrared (NIR) we selected  $\lambda = 900 \text{ nm}$  and the following parameters to match experiments performed by Huete, Jackson and Post (1985) :

**Table 2** Parameters used in radiosity calculation

Parameter	RED (650 nm)	NIR (900 nm)
$\rho$	0.0731	0.4661
$\tau$	0.0583	0.5000
$\rho_s$	0.33	0.3700

In Fig. 4 we show a scatter plot for the RED and NIR channel. Notice that in this representation the linear mixing model (eq. (17)) shows a nonlinear curvature because of the quadratic term of  $lai$  in eq. (17). Experimental results by Huete, Jackson and Post (1985) do not follow the curve of the linear mixing model and rather show a curve as predicted by the single-layer radiosity method. Note that Huete et al's data is expressed as green fractional green cover in percent. In order to compare a one-layer model to the measured data we

use the  $lai$  for one layer to represent the green fraction. In reality Huete et al's data was measured for layered canopies with a total  $lai$  from 0 to 4. In the hot spot direction the points between the 100 % soil and 100 % vegetation point (a layer of vegetation material without holes) describe an arc which is very similar to experiments performed by Roberts (1991). It is very interesting to note that Red/NIR scatter point for the radiosity model for a full leaf layer lies separated from the the simple linear mixing model. The radiosity derived reflectances lie close to a line connecting the 100 % leaf cover and 100 % soil points. The symbols denote measurements and computed red/nir reflectance for a fractional green cover or in our model for  $lai = 0., .2, .4, .6, .75, .9, 1..$  The spacing between the points decreases from a full vegetative cover to a bare soil and is very similar to reported experimental results by Huete, Jackson and Post (1985) and Satterwhite and Henley (1987) which are drawn in Fig. 4.

In Figure 5 we plot three vegetation indices :  $NDVI$ ,  $VI$  and  $SAVI$  for the above case. Note that the  $SAVI$  index is very similar for the radiosity derived indices for the hot spot and off hot spot direction. All used vegetation indices show quite large differences between the radiosity based nonlinear mixing model and the linear mixing model. For example the  $NDVI$  derived leaf area index with the simple mixture model is always about 0.2 larger than the radiosity based  $NDVI$ .

### 3 Radiosity Mixing Model for a Layered Canopy

In this section we use the previously derived analytical solution in Borel, Gerstl and Powers (1991) for the N-layer model to derive BRDF values. Each layer is characterized by its leaf area index  $lai$ , the leaf reflectance  $\rho$  and the leaf transmittance  $\tau$ . The ground has a reflection coefficient  $\rho_s$ . The upward radiance  $I_1^+$  above the top layer can then be used to compute the BRDF in the following way :

$$f(\theta_r \neq \theta_i, \phi_r \neq \phi_i) = \frac{I_1^+}{E_0} . \quad (18)$$

We have also shown that an analytical solution for the radiances  $I_n^+$  and  $I_n^-$ ,  $n = 1, 2, 3, \dots, N$  exists and has the form :

$$I_n^+ = C_1 (1 - b)^{n-1} + C_2 (1 + b)^{n-1}, \quad (19)$$



$$I_{N+1}^+ = \rho_s (C_3 (1 - b)^{N-1} + C_4 (1 + b)^{N-1}), \quad (20)$$

$$I_n^- = C_3 (1 - b)^{n-1} + C_4 (1 + b)^{n-1} - (1 - lai)^n E_0, \quad (21)$$

where  $C_1$ ,  $C_2$ ,  $C_3$ ,  $C_4$  and  $b$  are functions of  $\rho$ ,  $\tau$ ,  $\rho_s$ ,  $lai$  and  $E_0$ . These expressions can be evaluated very quickly and spectral radiances can be obtained at different levels inside the canopy. Figure 6 shows an example of spectral radiances as a function of the downward cumulative leaf area index and wavelength in a 30 layer canopy with a leaf area index of 0.1 per layer and the cotton reflectance and transmittance characteristics. It takes only about 2 seconds to compute all radiances for a 30 layer canopy and 140 different wavelengths on a UNIX workstation (SUN SparcStation IPC) using the computer language IDL.

### 3.1 Vegetation Indices for a Layered Canopy

As for the single-layer model we can show that vegetation indices are nonlinear functions of the total leaf area index. In Figure 7 we show a plot of the red and NIR reflectance of a 30-layer canopy as function of the total  $LAI$ . If we plot the data in a scatter diagram it follows the trend observed experimentally by Huete, Jackson and Post (1985). In Figure 8 we plot the three vegetation indices which have a steep rise for canopies with total  $LAI$ 's between 0. and 2. and then saturate. This leads us to conclude that vegetation indices such as  $NDVI$ ,  $VI$  and  $SAVI$  are useful for canopy  $LAI$  studies up to about 2, but do not change enough to allow the retrieval of the  $LAI$  of denser canopies ( $LAI > 2$ ). We expect that the use of radiosity based vegetation indices will improve the retrieval of  $LAI$  since multiple scattering and transmission are included. It might however be necessary to develop vegetation indices for various leaf angle distributions and sun angles.

### 3.2 Spectral BRDF for a Layered Canopy

For a layered canopy with  $N$  layers the spectral BRDF is given by the equation in Borel, Gerstl and Powers (1991)

$$f(\theta_i, \phi_i; \theta_r, \phi_r) = \frac{1}{E_0} \sum_{n=1}^{N+1} \frac{1}{\pi} [ P_n^{sunlit}(\theta_r, \phi_r) B_n^{sunlit} + P_n^{shade}(\theta_r, \phi_r) B_n^{shade} ], \quad (22)$$

where the radiosities  $B_n^{sunlit}$  are given by :

$$B_n^{sunlit} = \rho E_0 + B_n^{shade}, \quad n = 0, 1, \dots, N + 1 \quad (23)$$

and the radiosity in the shadow  $B_n^{shade}$  is given by :

$$B_n^{shade} = \begin{cases} (B_n^+ / lai) - \rho (1 - lai)^{n-1} E_0, & \text{if } n = 0, 1, \dots, N \\ B_n^+ - \rho_s (1 - lai)^n E_0, & \text{if } n = N + 1, \end{cases} \quad (24)$$

where the radiosity  $B_n^+$  is the layer-averaged radiosity of the upward pointing  $n$ -th leaf layer and can be determined using eq. (52) in Borel, Gerstl and Powers (1991) as :

$$B_n^+ = \begin{cases} \pi [I_n^+ - (1 - lai) I_{n+1}^+], & \text{if } n = 0, 1, \dots, N \\ \pi I_n^+, & \text{if } n = N + 1. \end{cases} \quad (25)$$

Using raytracing it is possible to compute the probabilities  $P_n^{sunlit}$  and  $P_n^{shade}$  for any illumination direction and view direction. For a 10 layer canopy with a layer  $lai$  of 0.1962 we computed the probabilities for an illumination direction of  $30^\circ$  and view angles from  $0^\circ$  to  $65^\circ$  in the principal plane. The probabilities are shown in Fig. 9. Notice that due to aliasing effects from the shadowing algorithm used by Borel (1988) the probability of seeing shadows is not equal to zero in the hot spot direction and also the probability of seeing a leaf is underestimated by about 25 %. The spectral BRDF for this simple canopy is shown in Fig 10. The soil constants were  $a = 0.2$  and  $b = 0.6$ . Notice the ridge produced by the hot spot effect for  $\theta_r = 30^\circ$ . We also found that the contrast ratio between the BRDF in the hot spot direction and zenith view angle :

$$C = \frac{f(\theta_i, \phi_i; \theta_i, \phi_i)}{f(\theta_i, \phi_i; \theta_r = 0^\circ, \phi_r = 0^\circ)}, \quad (26)$$

is strongly dependent on the wavelength as shown in Fig. 11. The contrast ratio seems to be proportional to  $(1 - \rho)$ , e.g. for a low reflectance the contrast ratio is larger than for high reflectances. This is due to the fact that shadows are relatively darker when the reflectance and transmittance are low and are brightened up due to multiple reflections and transmission of light when  $\rho$  and  $\tau$  are larger. We also computed the  $NDVI$  as a function of view angle and show the result in Fig. 12. The  $NDVI$  does not change much with the viewing angle for this relatively dense canopy. This is due to the fact that the BRDF for a horizontal Lambertian leaf canopy reaches an asymptote for viewing angles away from the hot spot. For less dense canopies the  $NDVI$  depends more on the viewing angle as one can deduce from the  $NDVI$  curves for the hot spot direction and the non-HS direction of Fig. 4.

## 4 Nonlinear Mixing for Rough Surfaces

In the previous sections we have shown that nonlinear mixing is due to multiple reflections and transmission of light. Another important case of nonlinear mixing occurs when materials with different spectral reflectances compose a rough surface, e.g. plowed field with exposed rocks or well mixed small particles of different minerals, see Singer and McCord (1979). In this section we develop simple models to illustrate the magnitude of nonlinear effects.

### 4.1 Two Facet Model

In Fig. 13 a simple geometry for one period in a periodic rough surface is shown. The surface extends to infinity in the direction vertical to the cross section. Each surface has a fraction  $f$  of material 1 and a fraction  $(1 - f)$  of material 2. The average reflectance  $\bar{\rho}$  per unit area is then given by :

$$\bar{\rho} = f \rho_1 + (1 - f) \rho_2 , \quad (27)$$

where  $\rho_1$  is the reflectance of material 1 and  $\rho_2$  is the reflectance of material 2. The radiosity equations for vertical illumination can then be written as :

$$\begin{aligned} B_1 &= \bar{\rho} E_0 \cos \theta + \bar{\rho} F_{12} B_2 \\ B_2 &= \bar{\rho} E_0 \cos \theta + \bar{\rho} F_{21} B_1 , \end{aligned} \quad (28)$$

where the view factors  $F_{12} = F_{21} = F$ . The view factor  $F$  between the surfaces can be determined by using the crossed string method, see Hottel and Sarofim (1967), which is illustrated in Fig. 14. The view factor between two infinite strips with areas  $S_1$  and  $S_2$ :

$$S_1 F_{12} = \frac{\overline{AD} + \overline{BC} - \overline{AC} - \overline{BD}}{2} , \quad (29)$$

where  $\overline{AD}$  is the length between the points  $A$  and  $D$ , etc. Thus we have :

$$F = (1 - \cos \theta) , \quad (30)$$

where  $\theta$  is the surface slope measured from the horizontal plane and the geometry is shown in Fig. 13. The solution of eq. (28) is then given by :

$$B = B_1 = B_2 = \frac{\bar{\rho} \cos \theta E_0 + \bar{\rho}^2 F \cos \theta E_0}{1 - \bar{\rho}^2 F^2} . \quad (31)$$

Next we need to determine the radiosity leaving the two facets. We can define an imaginary surface 3 covering the facets 1 and 2. Using the crossed string method the view factors between facets 1 and 2 to facet 3 are given by :

$$F_{31} = F_{32} = \frac{W + 2W \cos \theta - W}{2W} = \cos \theta , \quad (32)$$

and the radiosity over the two facets is then :

$$B_3 = B_1 F_{31} + B_2 F_{32} = 2 B W \cos \theta . \quad (33)$$

The reflectance of a periodic surface made of an infinite number of facets with illumination and view direction from nadir is then :

$$\begin{aligned} \rho_{radiosity}(\theta_i = 0, \phi_i = 0; \theta_r = 0, \phi_r = 0) &= \frac{B_3}{2 W \cos \theta E_0} = \frac{B}{E_0} \\ &= \frac{\bar{\rho} \cos \theta + \bar{\rho}^2 (1 - \cos \theta) \cos \theta}{1 - [\bar{\rho}(1 - \cos \theta)]^2}, \end{aligned} \quad (34)$$

where  $\rho_{radiosity}$  is the radiosity derived reflectance. For a linear mixing model the reflectance of a two component model is given by :

$$\rho_{linear} = \frac{\bar{\rho} \cos \theta E_0}{E_0} = \bar{\rho} \cos \theta . \quad (35)$$

## 4.2 Experimental Validation of the Two Facet Model

To validate the two facet model we built a mechanical model. An optical bench was used to hold two aluminum plates covered with colored paper and backed by black paper to eliminate possible multiple reflections between aluminum and paper. A fiberoptic spectrometer head was mounted on a copy stand and its field-of-view was carefully centered. The two facets were positioned towards the sun such that both faces were illuminated equally and specular reflections from the paper were kept as small as possible. The spectrometer was calibrated using a white calibration target which was put onto the edges of the two facets to measure  $E_0$ . The useful range of the spectrometer ranged from 400 nm to 900 nm with a spectral sample spacing of 1.4 to 1.5 nm. The angle  $\theta$  can be changed by sliding two holders on an optical bench into predetermined positions. The selected angles were  $\theta = 75^\circ, 65^\circ, 60^\circ, 50^\circ$  and  $36^\circ$ . Several colored papers and combinations of two different colored papers facing each other were measured. For each paper we measured the single surface reflectance  $\rho_{single}$  with the same spectrometer and an integrating sphere. To illustrate the nonlinear effect we

plot the multiple surface reflectance  $\rho_{multi}$  as a function of the slope corrected single surface reflectance  $\rho_{single} \cos \theta$ , see Fig. 15. In each plot we show three curves : measurement, radiosity computed (see eq. (34)) and linear mixing (see eq. (35)) for brown paper. No scaling or shifting was performed on the measured reflectances. This representation allows us to readily estimate the quantity by which the reflectance changes due to multiple reflections, e.g. for  $\theta = 75^\circ$  the multiple scattering component adds 0.5 to a single scattering contribution of 0.24 in the case of a single scattering reflectance of 0.9. Even for an angle of  $50^\circ$  the multiple scattering component is still greater than 0.25. The measurement and radiosity computed curves agree very well, except for  $\theta = 36^\circ$ . Eq. (34) can be solved for the slope angle  $\theta$  :

$$\theta(\rho_{single}, \rho_{multi}) = \cos^{-1} \left[ 1 - \frac{\rho_{single} - 1 + \sqrt{(1 + \rho_{single})^2 + 4\rho_{multi}(\rho_{multi} - \rho_{single} - 1)}}{2\rho_{single}(1 - \rho_{multi})} \right]. \quad (36)$$

Using eq. (36) and the measured single surface reflectances  $\rho_{single}$  and multi surface reflectances  $\rho_{multi}$  from 400 nm to 900 nm we compute the slope angle  $\theta$ . The averages for the estimated angles  $\langle \theta \rangle$  over the spectrum for the listed angles  $\theta$  are :  $73.67^\circ$ ,  $65.64^\circ$ ,  $55.46^\circ$ ,  $52.67^\circ$  and  $50.56^\circ$ . The average estimated angles are within  $5^\circ$  of the actual slope angles for the first four measurements and off by  $16^\circ$  for the fifth measurement. The differences could be due to mechanical problems, calibration problems, scattering from other surfaces, BRDF effects of the paper, etc. The conclusion of the experiment is however that indeed multiple scattering between bright surfaces will lead to nonlinear mixing and that the radiosity method can be used to predict the nonlinear effect.

The implications for geological remote sensing are that natural bright and very rough surfaces can have a very different spectrum than laboratory measured polished or smooth samples. It remains to be investigated how linear unmixing algorithms are affected by the nonlinear mixing.

### 4.3 Numerical Example of a Two-Component Surface

We calculated the reflectances  $\rho_{radiosity}$  and  $\bar{\rho}$  for two laboratory spectra (Goetz (1992)) for Alunite and Halloysite measured from  $0.3 \mu m$  to  $2.6 \mu m$  in steps of  $5 nm$ . We let the fraction  $f$  vary from 0 % to 100 % in steps of 33.33 % and set the slope angle to  $40^\circ$ . The resulting spectra are shown in Fig. 16. Notice the difference between the linear and the radiosity

based nonlinear mixing model. Note that even when only one material is present  $f = 0$ . and  $f = 1$ ., there is a difference in the spectra because of multiple reflections between the facets. We assume that the reflectance spectra used were measured for a flat sample.

#### 4.4 Numerical Example of a Three-Component Surface

It has been noted by several researchers e.g. Nash and Conel (1974); Hapke (1981) and Johnson, Smith, Taylor-George and Adams (1983) that nonlinear mixing occurs when spectra of well mixed or aggregates of minerals are measured. We can use the above model to study the behavior of the reflectance at particular wavelengths for a three component (ternary) surface. The average reflectance  $\bar{\rho}$  per unit area is then given by :

$$\bar{\rho} = f_1 \rho_1 + f_2 \rho_2 + (1 - f_1 - f_2) \rho_3, \quad (37)$$

where the fractions  $f_1$ ,  $f_2$  and  $(1 - f_1 - f_2)$  add up to unity. To demonstrate nonlinear mixing we selected laboratory spectra of Alunite, Halloysite and Kaolinite. The reflectance spectra as obtained from Goetz (1992) are shown in Fig. 17. To show that nonlinear mixing occurs we selected an absorption feature of Alunite and also Kaolinite at  $1.435 \mu m$  and one for Halloysite at  $1.91 \mu m$ . The slope was selected to be  $70^\circ$  to simulate thorough mixing, e.g. mixed powders as shown in Nash and Conel (1974). Figure 18 shows the reflectance in a triangle with the abundances of Kaolinite and Halloysite as x and y axes. Very similar nonlinear effects as in Nash and Conel (1974) are observed here. Extending the two and three component reflectance model to an N component model can be done as follows :

$$\bar{\rho} = \sum_{i=1}^N f_i \rho_i, \text{ where } \sum_{i=1}^N f_i = 1. \quad (38)$$

The reflectance of an N component surface is then obtained from eq. (34). We speculate that nonlinear effects have to be taken into account when spectral unmixing is done for wavelengths in absorption features. The nonlinear unmixing should be possible since only one additional parameter, the view factor  $F$  has to be determined. As we have noted earlier the view factor is related to the angle between the surface normal and nadir of the surface and thus could be used as a single parameter characterizing the surface roughness.

## 5 Conclusions

We have developed several simple models to demonstrate that nonlinear mixing occurs when multiple scattering effects are considered. First a one layer model of vegetation above ground was shown to exhibit an increased reflectance in the near infrared due to multiple reflections between the leaves and soil. The reflectance can double in our model calculations. Then we considered the effect of the nonlinear mixing on several vegetation indices and found a nonlinear relationship between vegetation indices and the leaf area index. We then turned to a layered canopy and showed that the up- and down-ward radiances inside a canopy have different spectral content. We found that vegetation indices for dense canopies are nonlinear with total  $LAI$ . Using a raytracing method to estimate probabilities for seeing illuminated and shaded leaves or ground we calculated the spectral BRDF for a slice in the principal plane. We also showed that the contrast ratio between the BRDF in the hot spot direction over the BRDF in the nadir direction is greatest for low reflectances and decreases for higher reflectances, e.g. in the green and near infrared. For a dense canopy we found that the NDVI depends weakly on the view angle.

A simple model for a rough surface composed of different minerals arranged on two tilted facets was developed. An experiment using two inclined paper facets illuminated by sunlight and a spectrometer measuring the reflectance in the visible and near infrared showed very good agreement between model and measurement. The reflectance of a two facet surface as a function of binary and ternary mixtures showed that multiple reflections change the shape of the spectrum where large reflectances occur and that intimate mixtures produce nonlinear mixing surfaces near absorption features.

Radiosity based models should be investigated in more detail theoretically and experimentally. Further investigations may lead to improved vegetation indices and possibly to nonlinear unmixing algorithms. The radiosity method is capable of modeling very complicated structures as shown in Borel, Gerstl and Powers (1991) and Goel, Rozehnal and Thompson (1991). Effects from scattered skylight should also be taken into account as well as atmospheric effects, see Huete and Jackson (1988). We believe that the extended radiosity, e.g. Borel and Gerstl (1991), could be used to model volumetric nonlinear mixing of plankton or sediments in water and possibly be applied to generate a biochemical

leaf reflectance scattering model. Further applications could lie in the modeling of multiple scattering between layered clouds and the ground surface. A possible application for Earth radiation budget sensors lies in better quantifiable fractional cloud covers.

A very important application for the near future lies in improving the vegetation indices for current sensors such as AVHRR and Landsat TM. We expect many new applications in the era of EOS for the planned high-resolution imaging spectrometers such as MODIS (Salomonson, Barnes, Maymon, Montgomery and Ostrow (1989)) and specially HIRIS (Goetz (1987) and Dozier and Goetz (1989)).

## Acknowledgment

*This research was supported by the Remote Sensing Science (RSS) Program under a project to investigate the applications of the radiosity method to remote sensing. We are grateful to Ghassem Asrar, Diane Wickland and Jon Ranson from NASA for their support. We thank Susan Ustin from the University of California at Davis for lending us her spectrometer and integrating sphere to perform the validation experiments. Karl Staenz from the Canadian Centre for Remote Sensing measured the cotton leaf reflectance and transmittance during the MAC-BRDF experiment in Maricopa, AZ. Finally we are extremely grateful to two summer students : Dirk-Udo Eisner and Jochen Glas from the Polytechnical University of Konstanz, Germany. Both designed and built the setup for the two facet experiment and measured the reported reflectances. We also acknowledge earlier contributions of Bill Powers, Los Alamos National Laboratory, to the analytical solution of the N-layer model.*



## References

- [1] G. Asrar. *Theory and Applications of Optical Remote Sensing*. Wiley, New York - Chichester - Brisbane - Toronto - Singapore, 1989.
- [2] F. Baret and G. Guyot. Potentials and limits of vegetation indices for LAI and APAR assessment. *Rem. Sens. Environ.*, 35:161–173, 1991.
- [3] C.C. Borel. *Models for Backscattering of Millimeter Waves from Vegetative Canopies*. PhD thesis, University of Massachusetts, September 1988.
- [4] C.C. Borel and S.A.W. Gerstl. Simulation of partially obscured scenes using the radiosity method. *Proc. SPIE*, 1486:271–277, April 1991.
- [5] C.C. Borel, S.A.W. Gerstl, and B.J. Powers. The radiosity method in optical remote sensing of structured 3-d surfaces. *Rem. Sens. Environ.*, 36:13–44, 1991.
- [6] J. Cihlar, L. St-Laurent, and J.A. Dyer. Relation between the normalized difference vegetation index and ecological variables. *Rem. Sens. Environ.*, 35:279–298, 1991.
- [7] J. Dozier and A.F.H. Goetz. HIRIS - EOS instrument with high spectral and spatial resolution. *Photogrammetria*, 43(3/4):167–180, 1989.
- [8] S.A.W. Gerstl and C.C. Borel. Principles of the radiosity method for canopy reflectance modeling. *Proc. Int. Geoscience and Remote Sensing Symposium*, 3:1735–1737, May 20-24 1990.
- [9] N.S. Goel. Models of vegetation canopy reflectance and their use in estimation of biophysical parameters from reflectance data. *Remote Sensing Reviews*, 4(1):221, 1988.
- [10] N.S. Goel, I. Rozehnal, and R.L. Thompson. A computer graphics based model for scattering from objects of arbitrary shapes in the optical region. *Rem. Sens. Environ.*, 36:73–104, 1991.
- [11] A.F.H. Goetz. High-resolution imaging spectrometer (HIRIS) - instrument panel report. *NASA, Earth Observation System Volume IIc*, 1987.

- [12] A.F.H. Goetz. SIPS user's guide : Version 1.2. *Report Center for the Study of Earth From Space (CSES), Univ. of Colorado*, page 89, September 1992.
- [13] R. O. Green. Proceedings of the third Airborne Visible/Infrared Imaging Spectrometer (AVIRIS) workshop. *JPL Publication 91-28*, May 20-24 1991.
- [14] B. Hapke. Bidirectional reflectance spectroscopy: 1. Theory. *J. Geophys. Res.*, 86(B4):3039–3054, April 1981.
- [15] H.C. Hottel and A.F. Sarofim. *Radiative Transfer*. McGraw-Hill Book Company, New York, New York, 1967.
- [16] A.R. Huete. Separation of soil - plant mixtures by factor analysis. *Rem. Sens. Environ.*, 19:237–251, 1986.
- [17] A.R. Huete and R.D. Jackson. Soil and atmosphere influences on the spectra of partial canopies. *Rem. Sens. Environ.*, 25:89–105, 1988.
- [18] A.R. Huete, R.D Jackson, and D.F. Post. Spectral response of a plant canopy with different soil backgrounds. *Rem. Sens. Environ.*, 17:37–53, 1985.
- [19] R.D. Jackson. Spectral indices in N-space. *Rem. Sens. Environ.*, 13:409–421, 1983.
- [20] M.F. Jasinski. Sensitivity of the normalized difference vegetation index to subpixel canopy cover, soil albedo, and pixel scale. *Rem. Sens. Environ.*, 32:169–187, 1990.
- [21] P.E. Johnson, M.O. Smith, S. Taylor-George, and J.B. Adams. A semiempirical method for analysis of the reflectance spectra of binary mineral mixtures. *J. Geophys. Res.*, 88:3557–3561, 1983.
- [22] R.J. Kauth and G.S. Thomas. The tasseled cap - a graphic description of the spectral-temporal development of agricultural crops as seen by Landsat. *Proc. Symp. on Machine Proc. of Remotly Sensed Data, Purdue Univ., West Lafayette, IN*, pages 41–51, 1976.
- [23] D.B. Nash and J.E. Conel. Spectral systematics for mixtures of powdered Hypersthene, Labradorite and Ilmenite. *J. Geophys. Res.*, 79(11):1615–1621, April 1974.
- [24] D.A. Roberts. *Separating Spectral Mixtures of Vegetation and Soils*. PhD thesis, University of Washington, June 1991.

- [25] D.A. Roberts. *Private Communication*, 1992.
- [26] D.A. Roberts, J.B. Adams, and M.O. Smith. Predicted distribution of visible and near-infrared radiant flux above and below a transmittant leaf. *Rem. Sens. Environ.*, 34:1–17, 1990.
- [27] D.A. Roberts, M.O. Smith, J.B. Adams, and A.R. Gillespie. Leaf spectral types, residuals, and canopy shade in an AVIRIS image. *Proc. 3<sup>rd</sup> Airborne Visible/Infrared Imaging Spectrometer (AVIRIS) Workshop*, (JPL Publication 91-28):43–50, May 20-21 1991.
- [28] H.E. Rushmeier and K.E. Torrance. The zonal method for calculating light intensities in the presence of a participating medium. *SIGGRAPH Proceedings*, 21(4):293, July 1987.
- [29] V.V. Salomonson, W.L. Barnes, P.W. Maymon, H.E. Montgomery, and H. Ostrow. MODIS : Advances facility for studies of the Earth as a system. *Trans. on Geoscience and Remote Sensing*, 27(3):145–153, 1989.
- [30] M.B. Satterwhite and J.P. Henley. Spectral characteristics of selected soils and vegetation in nothern nevada and their discrimination using band ratio techniques. *Rem. Sens. Environ.*, 23:155–175, 1987.
- [31] R.B. Singer and T.B. McCord. Mars: Large scale mixing of bright and dark surface materials and implications for analysis of spectral reflectance. *Proc. Planet. Sci. Conf.*, 10<sup>th</sup>, 2:1835–1848, 1979.
- [32] M.O. Smith, S.L. Ustin, J.B. Adams, and A.R. Gillespie. Vegetation in deserts: I A regional measure of abundance from multispectral images. *Rem. Sens. Environ.*, 31:1–26, 1990.
- [33] M.O. Smith, S.L. Ustin, J.B. Adams, and A.R. Gillespie. Vegetation in deserts: II Environmental influences on regional abundance. *Rem. Sens. Environ.*, 31:27–52, 1990.
- [34] K. Staenz. Licor measured conical/bi-hemispherical spectral reflectance and transmittance spectra of cotton. *Private Communication*, 1991.
- [35] C.J. Tucker. Red and photographic infrared linear combinations to monitor vegetation. *Rem. Sens. Environ.*, 8:127–150, 1979.

- [36] G. Vane and A.F.H. Goetz. Terrestrial imaging spectroscopy. *Rem. Sens. Environ.*, 24:1–29, 1988.
- [37] D.L. Williams. A comparison of spectral reflectance properties at the needle, branch and canopy level for selected conifer species. *Rem. Sens. Environ.*, 35:79–93, 1991.

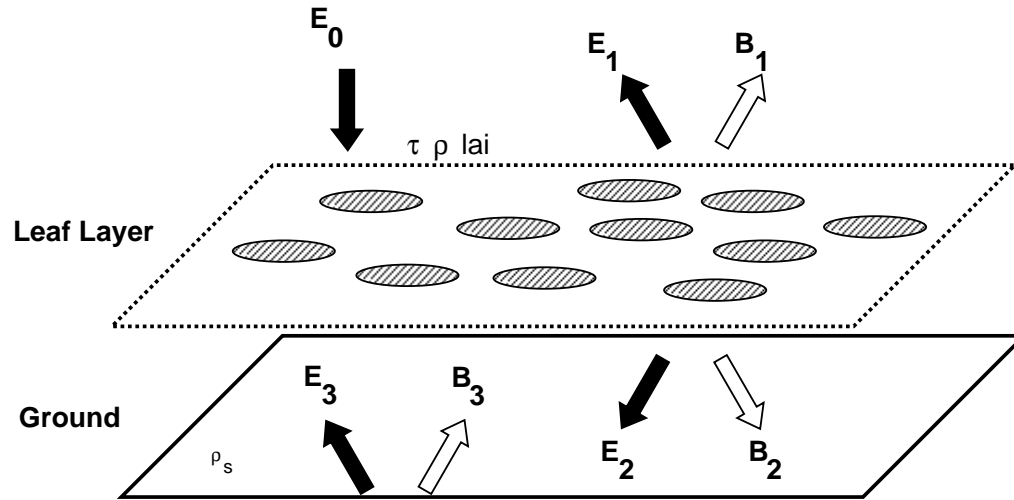


Figure 1: Geometry for a single-layer of horizontal and non-overlapping Lambertian disks above a Lambertian reflecting surface. The black arrows indicate the single scattering components  $E$  and the white arrows indicate the radiosities  $B$ .

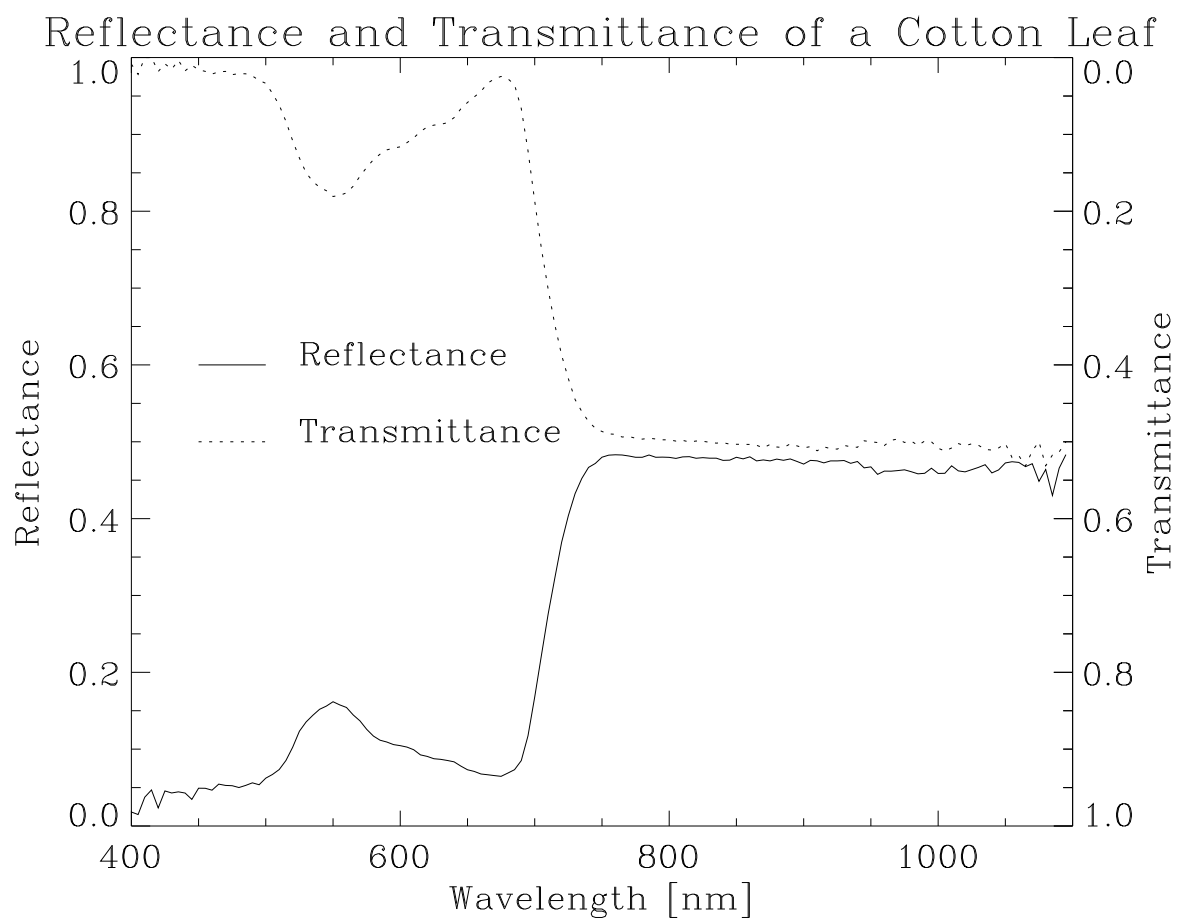


Figure 2: Reflectance and transmittance of a mature Cotton leaf (note the different axes for  $\rho$  and  $\tau$ ).

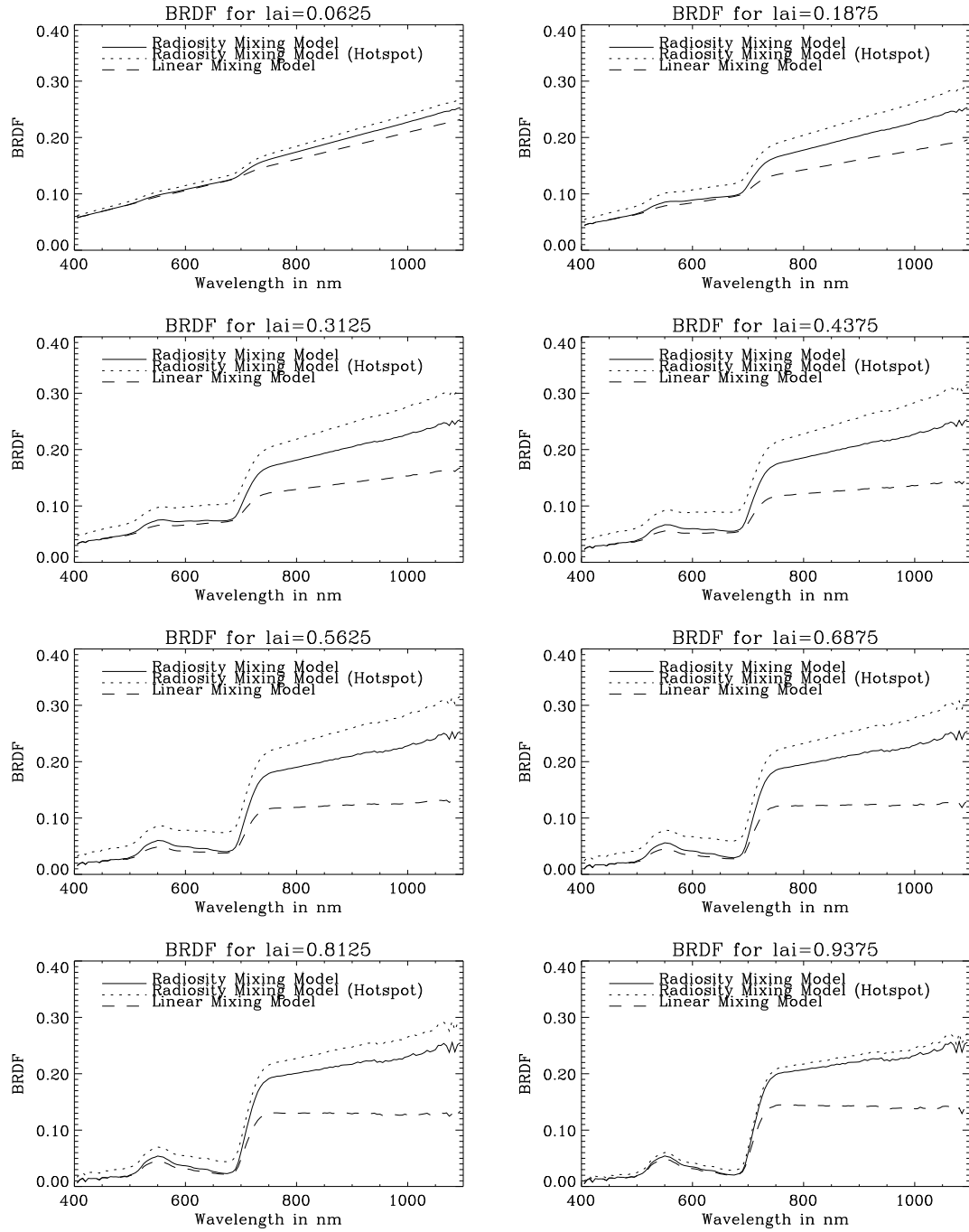


Figure 3: Spectral BRDF for a single-layer canopy above ground as a function of leaf area index.

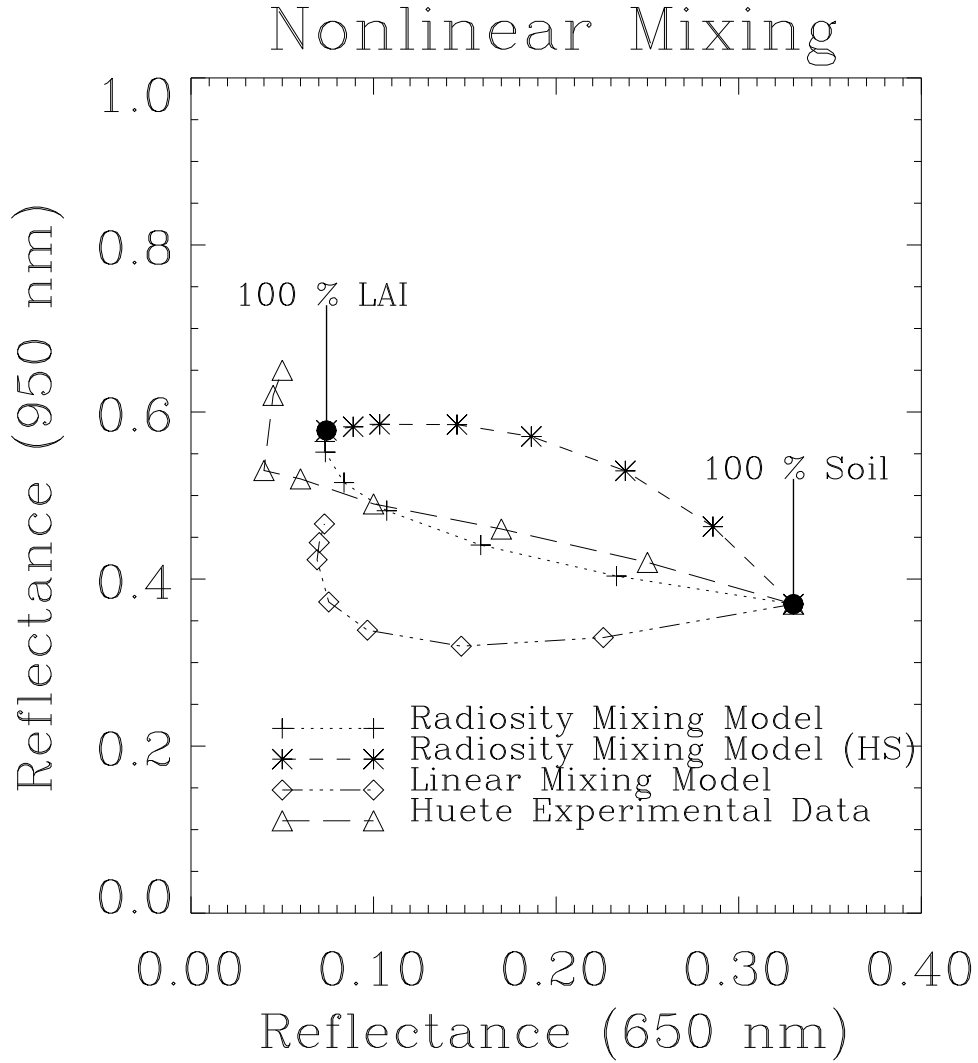


Figure 4: Scatter plot for red and near infrared channel as a function of the green cover fraction or in the case of the single layer model the leaf area index in steps of 0 %, 20 %, 40 %, 60 %, 75 %, 90 %, 95 % and 100 % and compared to measured data from Huete, Jackson and Post (1985).



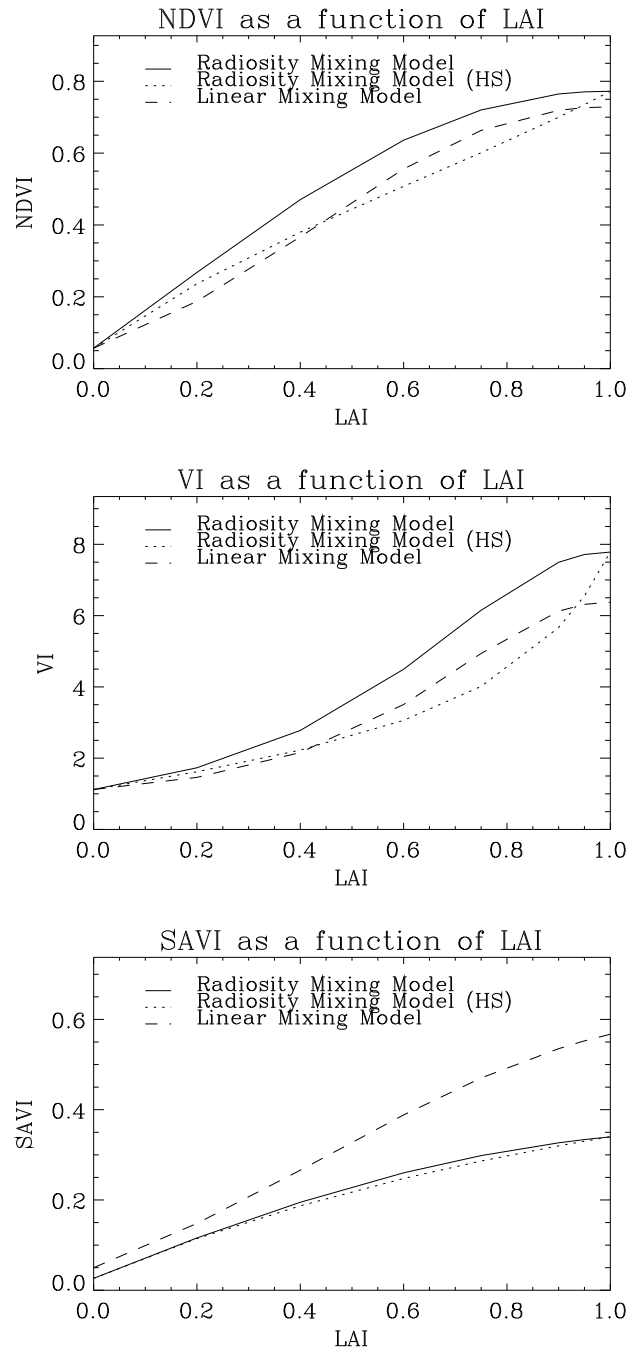


Figure 5: Three vegetation indices as a function of  $LAI$  for soil coefficients  $a = 0.2$  and  $b = 0.6$ .

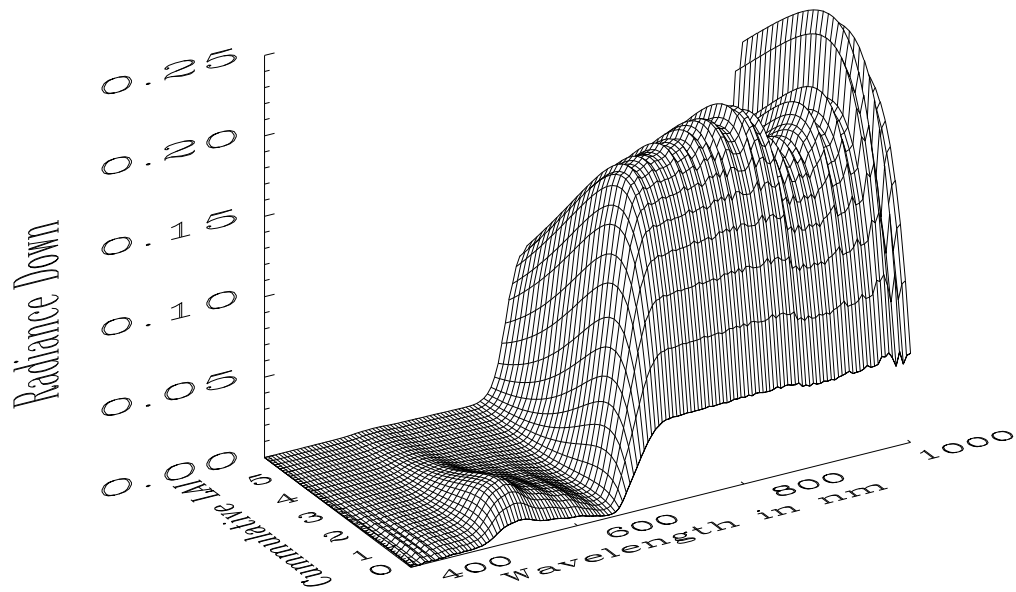
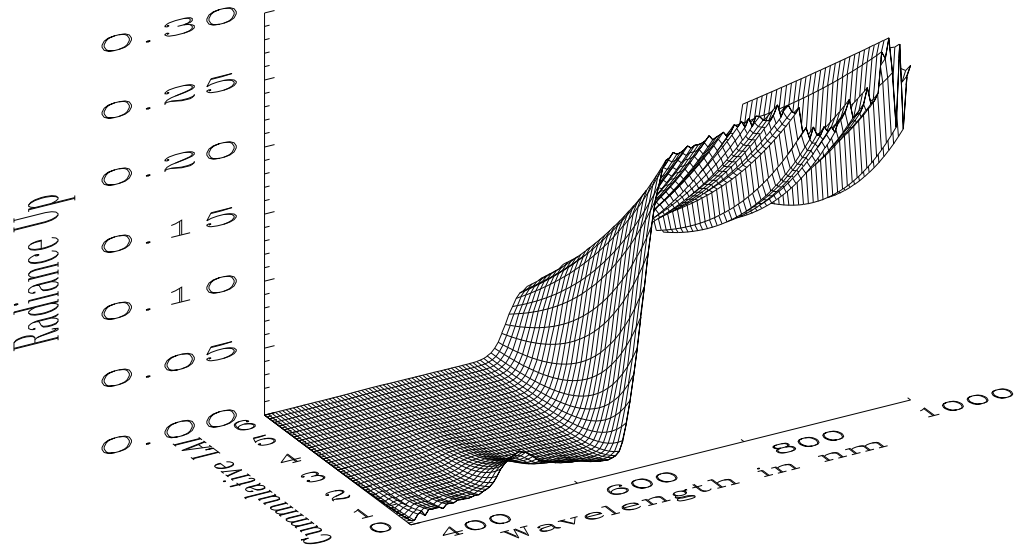


Figure 6: Spectral up- and down radiances inside a 30 layer canopy with a leaf area index of 0.1 per layer and soil coefficients  $a = 0.2$  and  $b = 0.6$ .

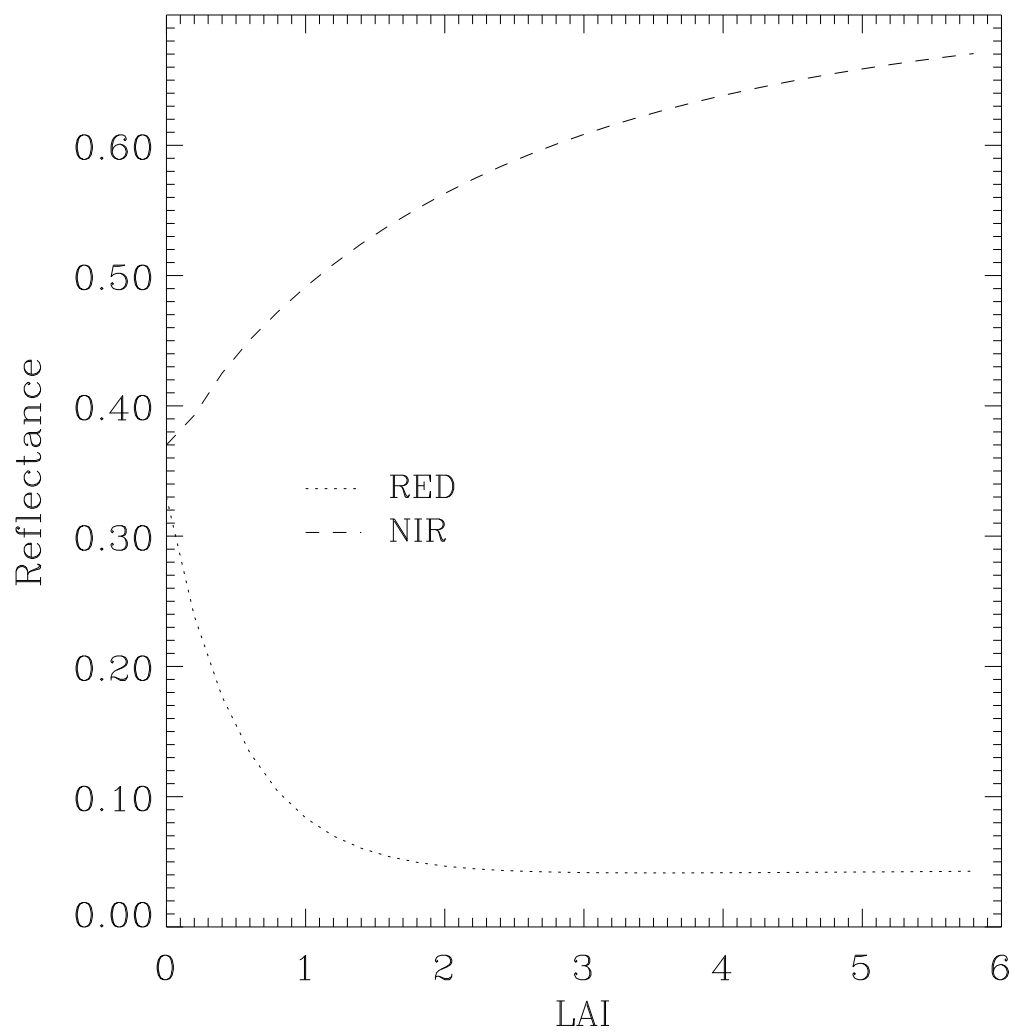


Figure 7: Red and NIR Reflectance for a 30-layer canopy as a function of the total leaf area index.

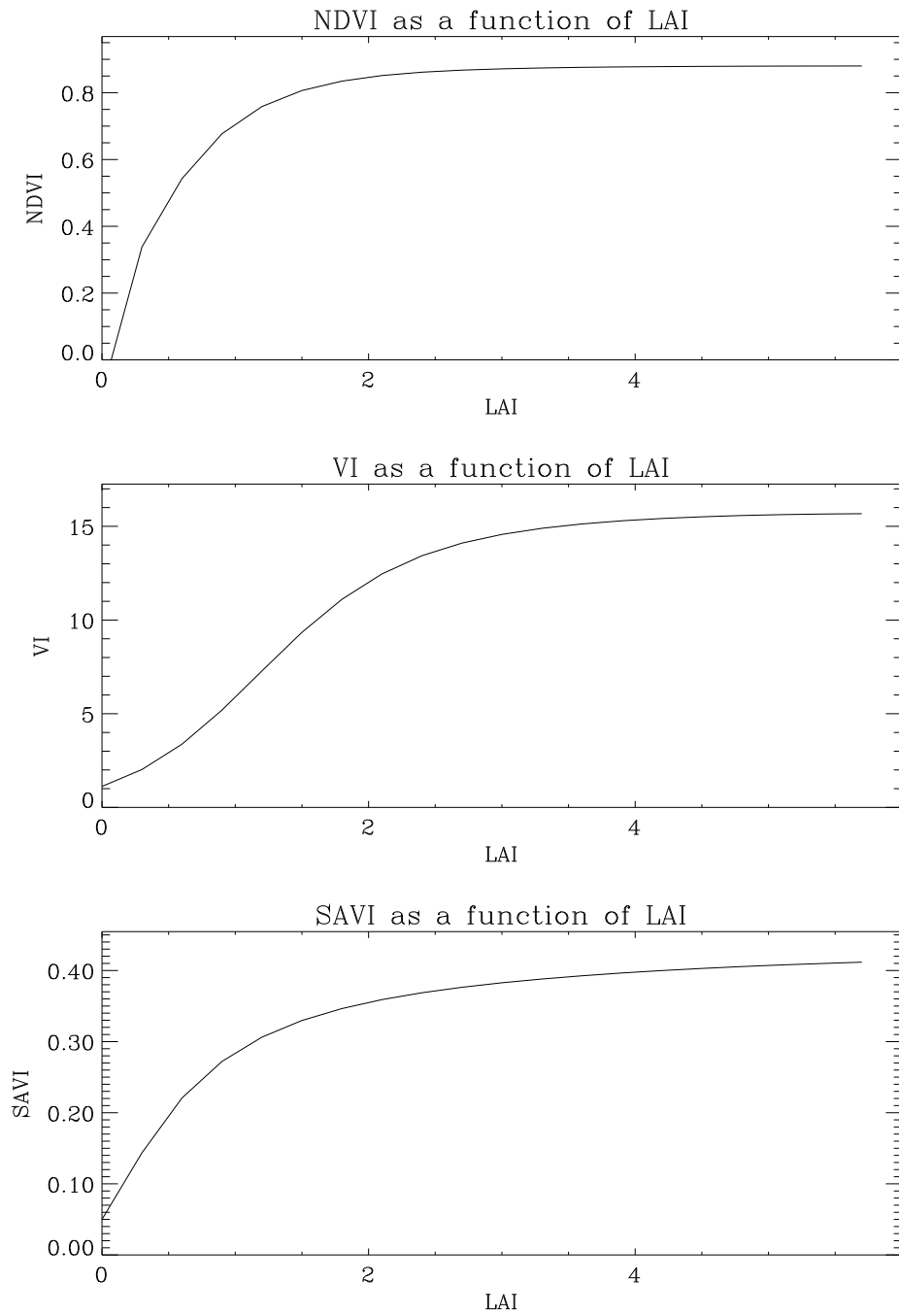


Figure 8: Three vegetation indices as a function of the total leaf area index of a 30 layer canopy for soil coefficients  $a = 0.2$  and  $b = 0.6$ .

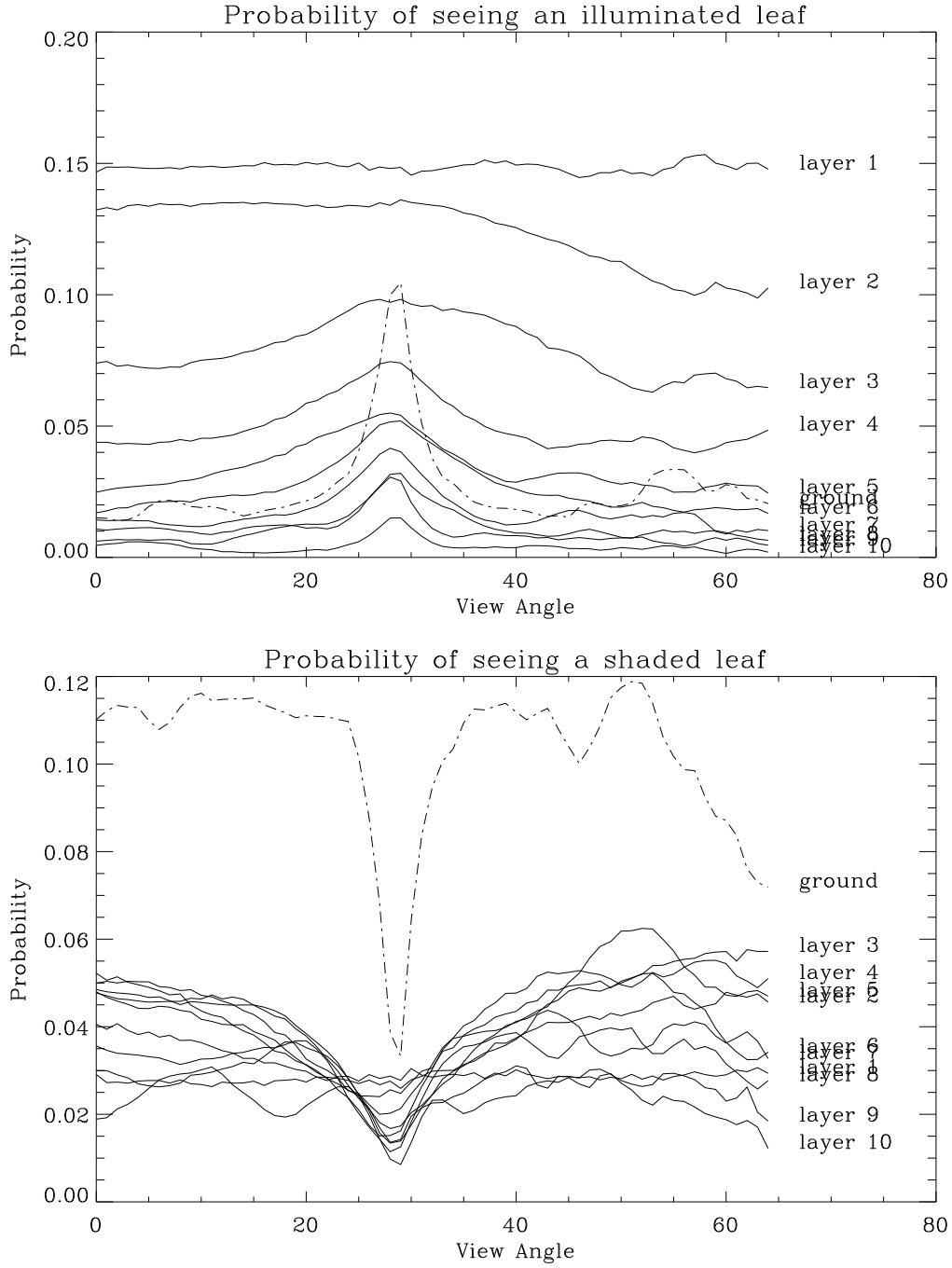


Figure 9: Probabilities of seeing sunlit and shaded leaves and ground as a function of view angle for a illumination direction of  $30^\circ$  in the principal plane.

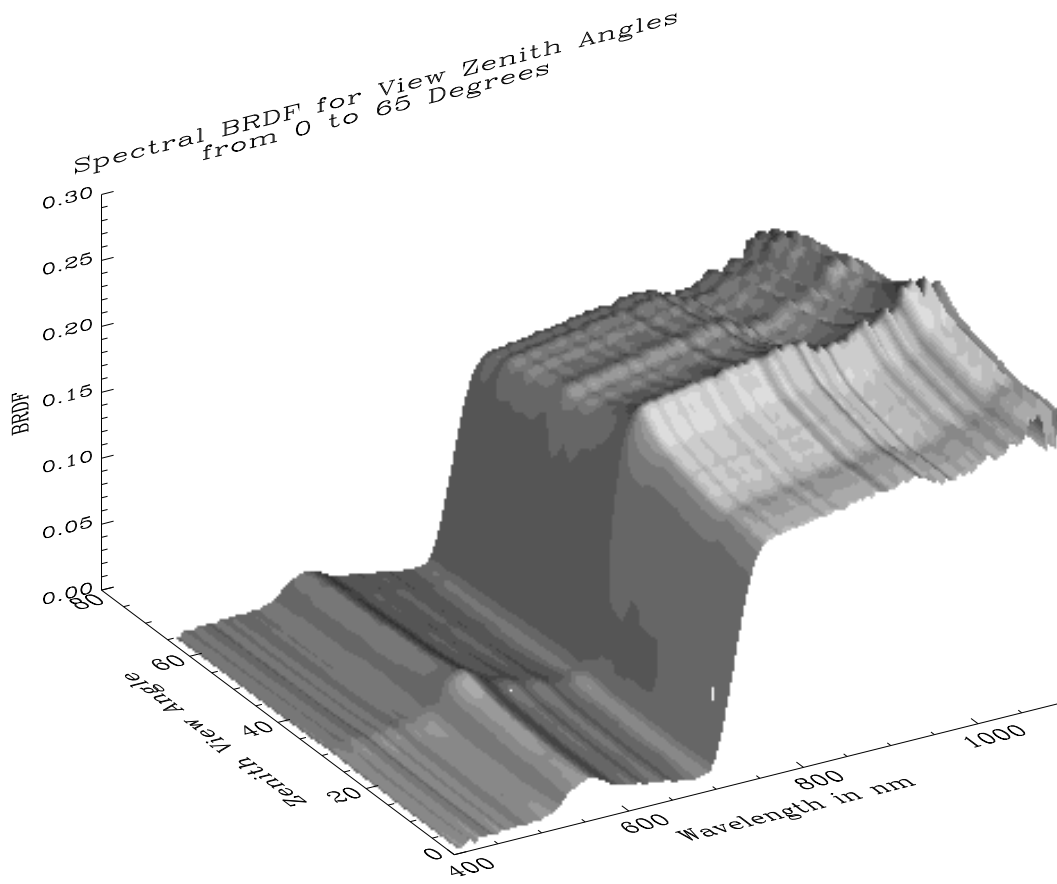


Figure 10: Spectral BRDF for a 10 layer canopy with a total  $LAI = 1.962$ .

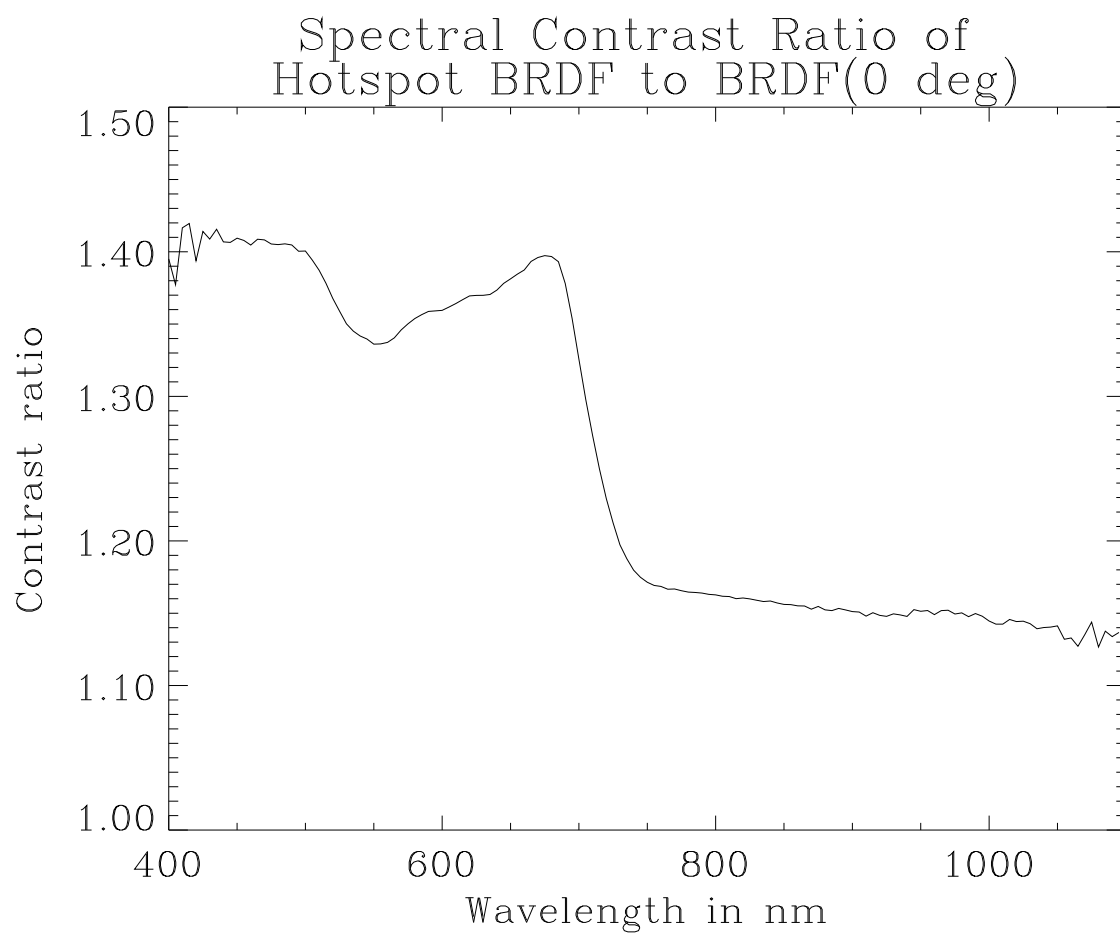


Figure 11: Contrast ratio as a function of wavelength for a 10 layer canopy with a total  $LAI = 1.962$ .

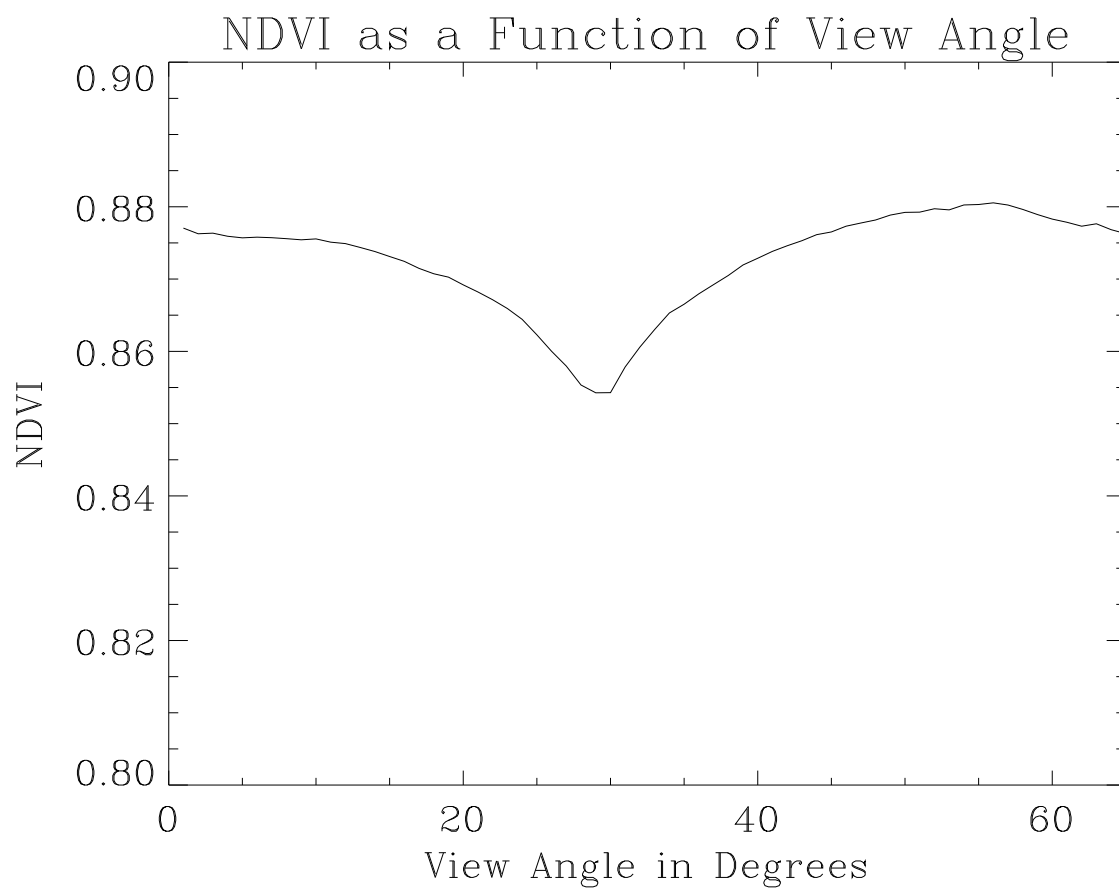


Figure 12: NDVI as a function of view angle.



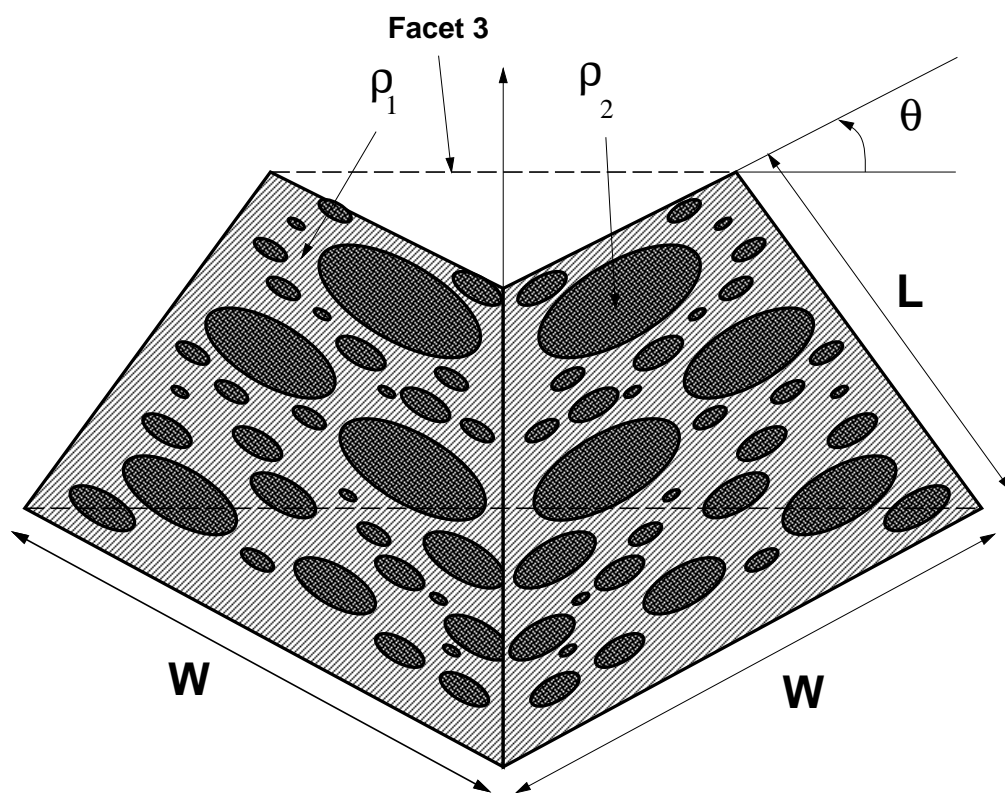


Figure 13: Geometry of a rough surface composed of two materials.

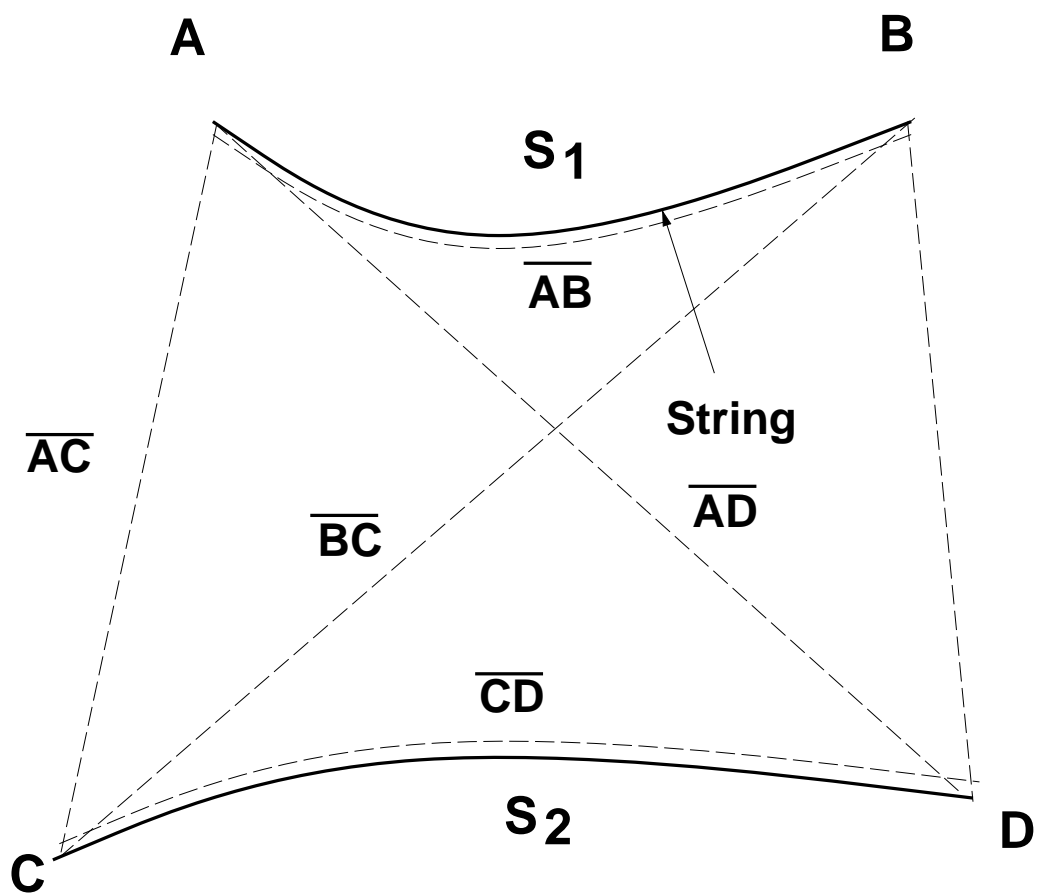


Figure 14: Crossed string method to compute view factors.

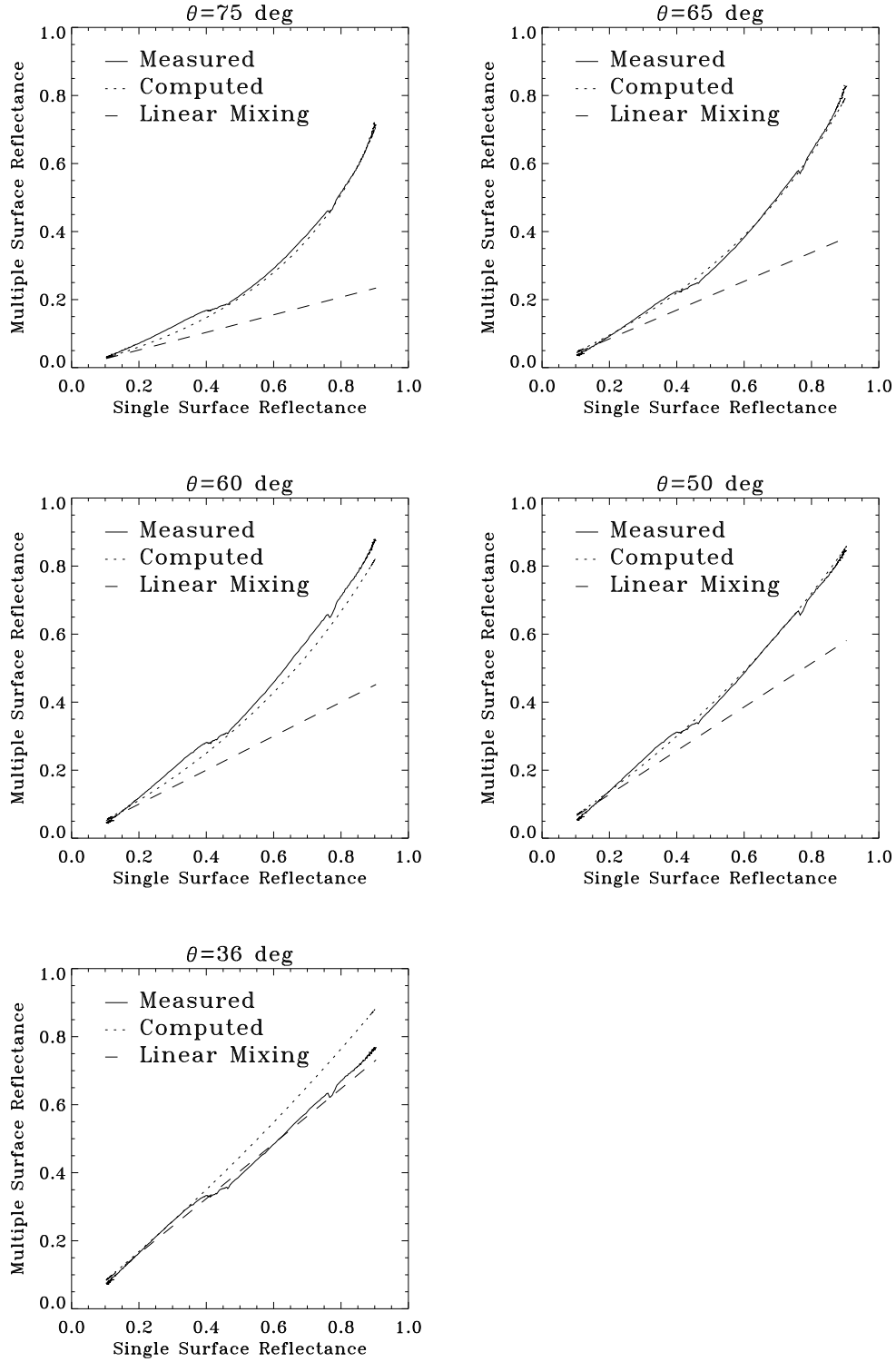


Figure 15: Multiple surface reflectance versus single surface reflectance of a two-facet structure. Each plot shows measured, radiosity computed and linear mixing model curves for facet angles :  $\theta = 75^\circ$ ,  $65^\circ$ ,  $60^\circ$ ,  $50^\circ$  and  $36^\circ$  and brown paper.

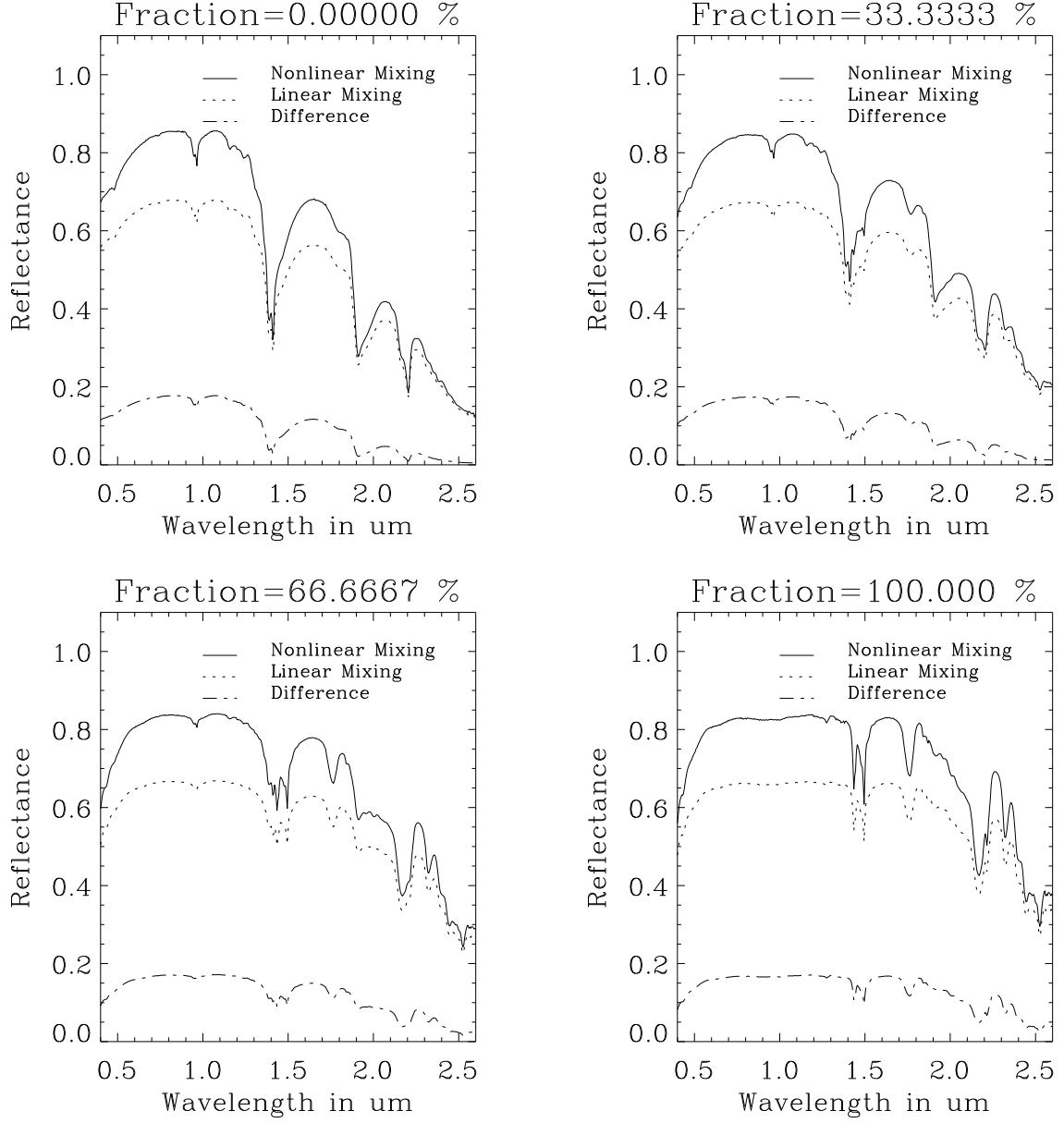


Figure 16: Spectra of mixtures of Alunite and Halloysite in a sloped surface model  $\theta = 40^\circ$  as fractions of Halloysite (0 %, 33.3 %, 66.6 % and 100 %).

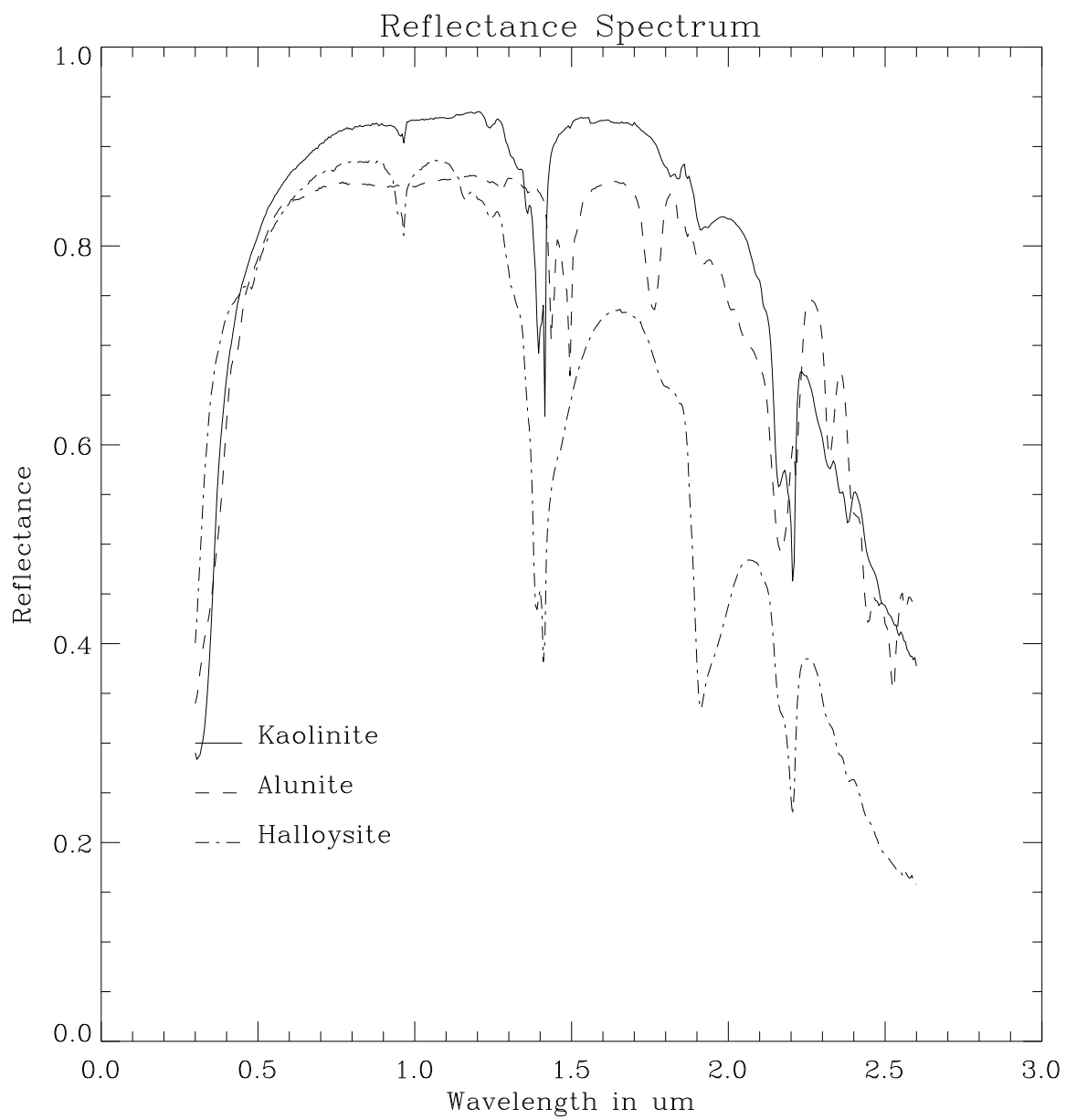


Figure 17: Reflectance spectra of Alunite, Halloysite and Kaolinite minerals.

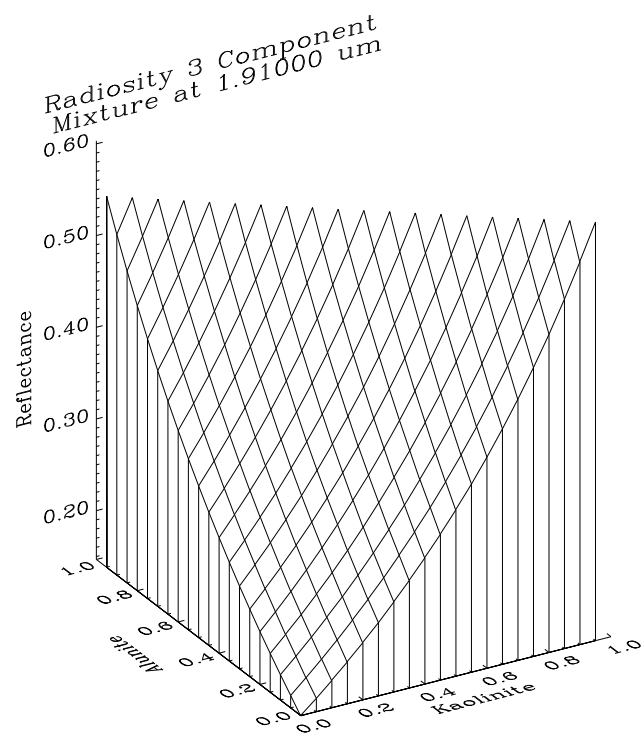
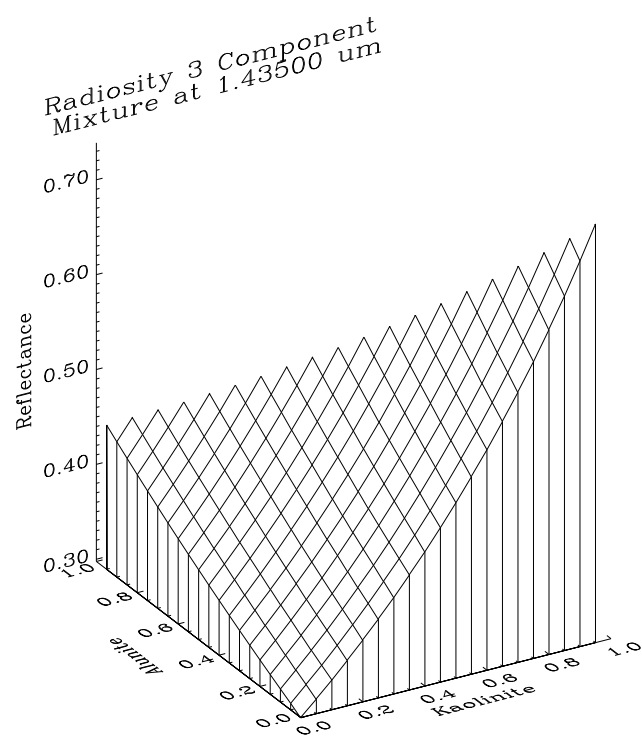


Figure 18: Reflectance for a ternary mixture of Alunite, Halloysite and Kaolinite at selected wavelengths for  $\theta = 70^\circ$ .